A&A 424, L9–L12 (2004)
DOI: 10.1051/0004-6361:200400036

Astronomy & Astrophysics

Letter to the Editor

The clustering of ultraviolet-selected galaxies at $z \approx 0.1$

S. Heinis[1], M. Treyer[1], S. Arnouts[1], B. Milliard[1], J. Donas[1], R. Gal[2], D. C. Martin[3], and M. Viton[1]

[1] Laboratoire d'Astrophysique de Marseille, BP 8, Traverse du Siphon, 13376 Marseille Cedex 12, France
e-mail: Sebastien.Heinis@oamp.fr
[2] UC Davis, Department of Physics, One Shields Ave., Davis, CA 95616, USA
[3] California Institute of Technology, MC 405-47, 1200 East California Boulevard, Pasadena, CA 91125, USA

Received 4 February 2004 / Accepted 14 July 2004

Abstract. We present the first angular clustering measurement of ultraviolet-selected galaxies at low redshift ($z \approx 0.1$) using data from the FOCA survey. We measure the galaxy autocorrelation function $\omega(\theta)$ from three separate fields with $m_{\rm UV} < 20.25$ (AB). Assuming $\omega(\theta) = A_\omega \theta^{-\delta}$, we obtain $A_\omega = 2.9^{+1.9}_{-1.2} \times 10^{-2}$ and $\delta = 0.53^{+0.23}_{-0.26}$, as a best fit to the data, which yields a correlation length $r_0 = 3.2^{+0.8}_{-2.3}\ h^{-1}$ Mpc. This estimate is formally lower than those obtained from optically selected $L_\star$ galaxy samples, although the difference is within errors.

Key words. ultraviolet: galaxies – cosmology: large-scale structure of Universe

1. Introduction

Observational evidence of the decline of star formation (SF) from $z = 1$ to $z = 0$ has been accumulating in recent years (e.g. Lilly et al. 1996; Madau et al. 1998; Cowie et al. 1999). However, the mechanisms causing this rapid decline are still poorly understood. In particular, it has been suggested by hydrodynamic simulations that large-scale environmental effects could play a key role in regulating SF (e.g. Blanton et al. 1999; Nagamine et al. 2000; Yoshikawa et al. 2001): while at high redshift the bulk of SF is expected to take place in high-density regions, the heating of the gas in these regions could subsequently inhibit SF, making lower density regions preferred sites for SF as redshift decreases. Observationally, hints for such behavior in the local universe were found by Gómez et al. (2003) using an optically selected sample of galaxies. Another approach is to compare the clustering properties of UV-selected, star-forming galaxies with those of the global galaxy population as well as those of the underlying dark matter. At high redshift, the clustering properties of Lyman break galaxies (rest-frame UV selected) show that these preferentially populate regions of high dark matter density (e.g. Giavalisco & Dickinson 2001; Arnouts et al. 2002; Foucaud et al. 2003), and that the clustering increases with rest-frame UV luminosity (Giavalisco & Dickinson 2001). On the other hand, there is evidence that local star-forming galaxies, selected by spectral types or colors, are less clustered than the old, passively evolving population (Madgwick et al. 2003; Zehavi et al. 2002).

In this work, we present the first clustering measurement of local UV-selected galaxies using data from the FOCA experiment (Milliard et al. 1991). After separating stars from galaxies (Sect. 2.1), we compute the angular autocorrelation function (ACF) (Sect. 3). In Sect. 3.3, we derive the value of the correlation length and in Sect. 4 we compare it with previous results both in the local Universe (based on optical samples) and at high z (rest-frame UV selected samples). Throughout this paper, we assume a Λ-flat cosmology with $\Omega_0 = 0.3$, $\Omega_\Lambda = 0.7$, $H_0 = 100\,{\rm km\,s^{-1}\,Mpc^{-1}}$.

2. The survey datasets

We use three fields observed with the balloon-borne FOCA imager at an effective wavelength of 2015 Å. Each pointing covers a circular field of view with a diameter of 1.55°. Table 1 shows the central coordinates of the fields, the number of sources down to $m_{\rm UV} < 20.25$, and the properties of the spectroscopic sample obtained in two of the three fields (Treyer et al. 1998; Sullivan et al. 2000; Zappelli 2001). The UV flux has been corrected for galactic extinction using dust maps from Schlegel et al. (1998) and converted to the AB system. Optical counterparts have been assigned by cross-matching with the *gr* data from DPOSS (Gal et al. 2003) (there is no SDSS overlap) using a search radius of 6 arcsec. 64% of the sources in the three fields (Col. 4 of Table 1) have a unique optical counterpart. For those with multiple counterparts, we selected the brightest g-band detection, which is also the closest match in 95% of the cases. We rejected those UV detections with no optical counterpart within our search radius (≈16%), as we found through visual inspection that the majority (65%) of them are spurious detections, with the remainder being bright stars which are saturated in the DPOSS.

Table 1. Description of the sample ($m_{\rm UV} < 20.25$): field name (1); field center coordinates (J2000) (2) and (3); number of sources with a DPOSS counterpart within 6 arcsec (4); number of spectroscopic galaxies (excluding cluster members) (5); number of spectroscopic stars (6); number of galaxies after star/galaxy separation (7).

Field	RA	Dec	DPOSS	z-gal.	z-stars	Color-selected galaxies
Q030	13 06 10.43	+29 01 46.1	262	118	28	162
Q089	15 38 59.64	+34 41 25.1	284	44	32	187
Q097	13 32 09.66	+47 14 17.6	214	–	–	124

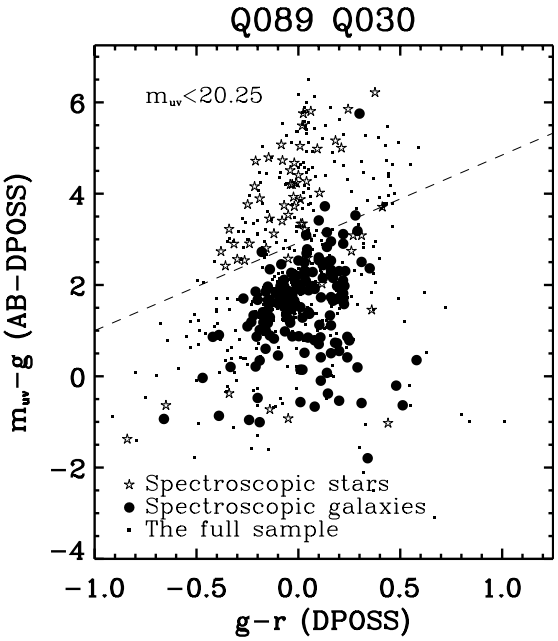

Fig. 1. $(\mathrm{UV}-g)$ vs. $(g-r)$ color–color diagram for the FOCA sources. The filled circles and stars represent the spectroscopically confirmed galaxies and stars, respectively. Dots are the UV detections with a DPOSS counterpart. The line is: $(m_{\rm UV} - g) = 1.92 * (g - r) + 2.92$.

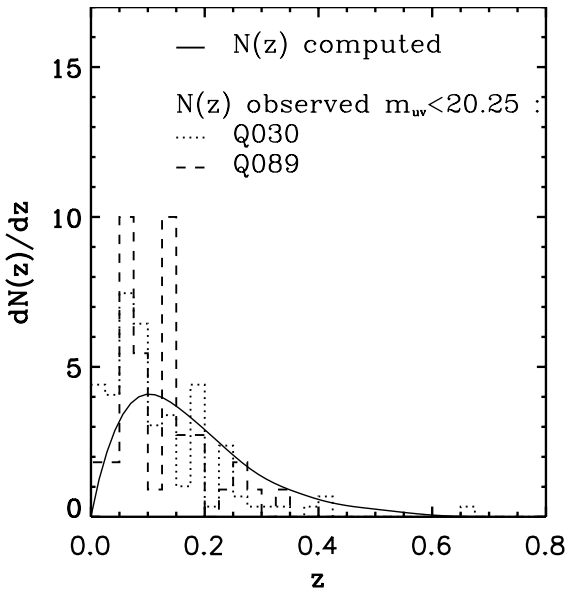

Fig. 2. The normalized redshift distributions for spectroscopically confirmed galaxies. The dotted and dashed lines are the observed $N(z)$ in Q030 and Q089, respectively; the solid line is the modeled $N(z)$ (see Sect. 2.2 for details).

2.1. Star/galaxy separation

Star-galaxy separation was performed using the $(\mathrm{UV} - g)$ vs. $(g - r)$ color–color diagram. We used the spectroscopic sample to derive a simple color criterion (the dashed line in Fig. 1) whereby 96% of the spectroscopic galaxies are recovered, with 10% contamination by spectroscopically confirmed stars. This criterion was then applied to the full sample in order to derive a galaxy sample, from which we further excluded the spectroscopic quasars as well as the spectroscopic cluster members (Coma in Q030 (SA57), see Treyer et al. (1998); Sullivan et al. (2000); and Abell 2111 in Q089, Zappelli (2001)). The exclusion of these objects has negligible impact on our results. Our final sample consists of 473 galaxies (Col. 7 in Table 1).

2.2. The redshift distribution

Figure 2 shows the observed redshift distribution in the 2 fields with spectroscopic followup (dashed and dotted lines). The mean redshift is ≈0.1. The observed redshift distribution of the Q089 field shows two strong features, the one at $z \approx 0.07$ likely corresponding to the outskirts of the Corona Borealis Supercluster (Small et al. 1997). The solid line shows the model distribution using the luminosity function derived by Sullivan et al. (2000) and assuming a mean Sd-type k-correction (Coleman et al. 1980).

3. The angular correlation function and correlation length

3.1. The angular correlation function: $\omega(\theta)$

To measure $\omega(\theta)$, we used the estimator proposed by Landy & Szalay (1993), which has a nearly Poissonian variance. We used a logarithmic bin: $\Delta \log \theta = 0.4$ with minimum and maximum angular separations of $\theta = 0.015$ and $0.5°$ respectively.

We processed the three fields as a single, non-contiguous field, which minimizes the integral constraint correction. Our result is shown in the top panel of Fig. 3. The θ value considered is the average separation in each bin.

3.2. The amplitude and slope: A_ω and δ

We fit our angular clustering measurement with a power-law using the usual formalism: $\omega(\theta) = A_\omega \theta^{-\delta}$. To do so, we carried out a first χ^2 minimization using Poissonian errors. This best fit was then used to estimate the total errors using Bernstein's equation (Bernstein 1994) as applied in Arnouts et al. (2002)

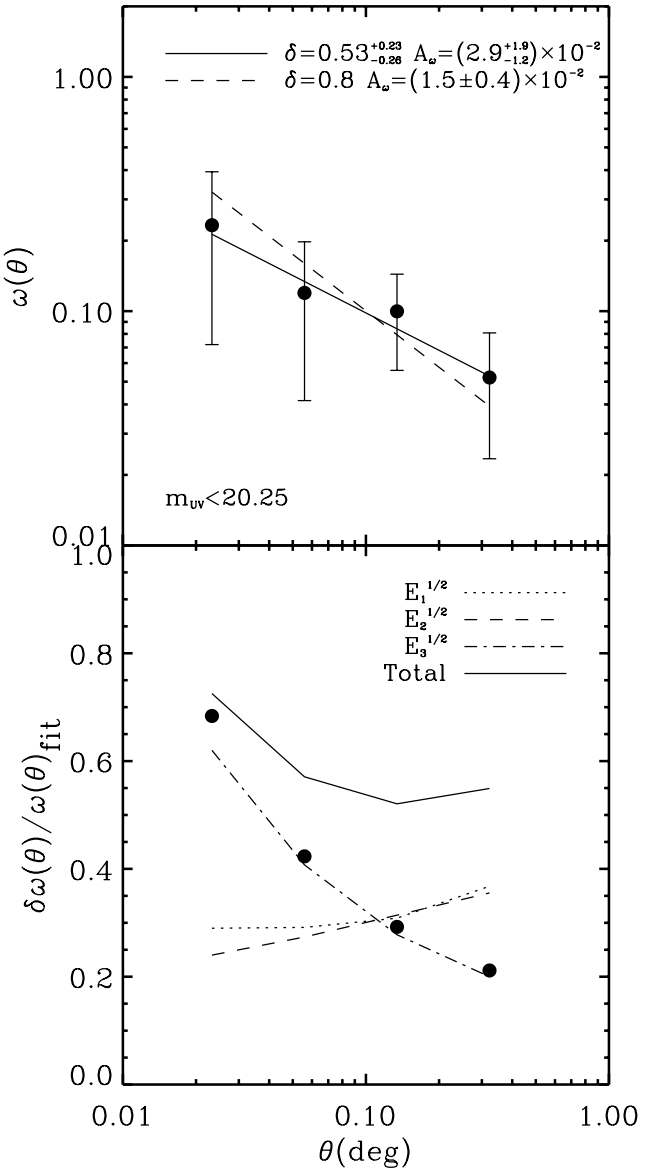

Fig. 3. *Top panel*: the measured autocorrelation function of our UV-selected sample (filled circles). The errors are as described in Sect. 3.2. The solid line shows the best power-law fit to the measurements, while the dashed line shows the best fit using $\delta = 0.8$. *Bottom panel*: comparison of Poissonian errors (filled circles) and cosmic uncertainties computed using Eq. (38) of Bernstein (1994).

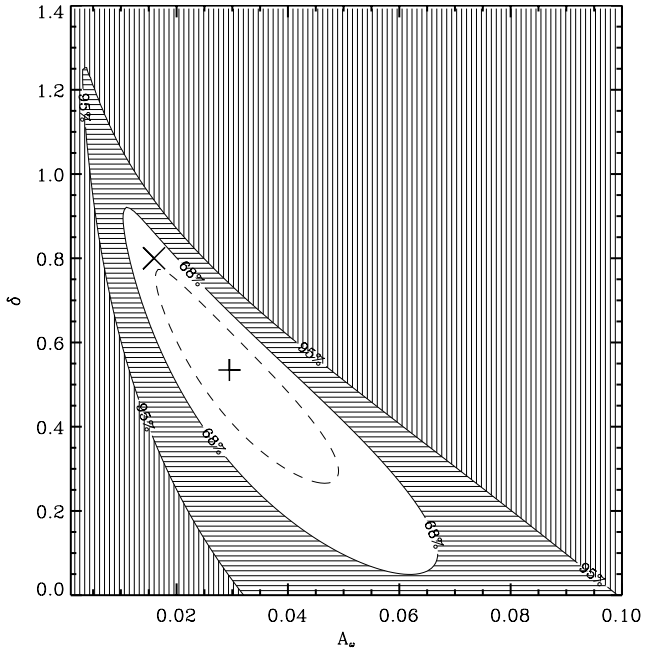

Fig. 4. Contours of constant χ^2 in the (A_ω, δ) parameter space: the inner and outer solid lines correspond to the 68.3% and 95.4% confidence levels, respectively. The dashed line corresponds to the ($\chi^2_{\rm min}$ + 1) level. The + sign shows the best fit amplitude and slope; the cross indicates the best fit amplitude assuming $\delta = 0.8$.

with a zero bias model. The results are shown in the bottom panel of Fig. 3. The Poisson errors are well described by the E_3 term, which dominates the error budget at small separations. However, at large scales the cosmic variance (i.e., the finite volume error, E_1) and the discreteness error (E_2) dominate and the total error is underestimated by the Poissonian approximation. The final fitting was performed using the total errors ($E^{1/2} = (E_1 + E_2 + E_3)^{1/2}$).

We derive $A_\omega = (2.9^{+1.9}_{-1.2}) * 10^{-2}$ and $\delta = 0.53^{+0.23}_{-0.26}$ (solid line in Fig. 3, top panel), and $A_\omega = (1.5 \pm 0.4) * 10^{-2}$ for a fixed slope $\delta = 0.8$. (dashed line), with θ in degrees. We determined the error bars on A_ω and δ using the projected ($\chi^2_{\rm min}$ + 1) contour (Fig. 4). The 68.3% and 95.4% confidence levels are also shown (the inner and outer solid lines respectively).

3.3. The correlation length: r_0

We derived the comoving correlation length, r_0, from the best fit amplitude and slope of $\omega(\theta)$ using the Limber equation (see for example Peebles 1980) with the modeled redshift distribution (Sect. 2.2). We obtain $r_0 = 3.2^{+0.8}_{-2.3}\ h^{-1}$ Mpc in the case where A_ω and δ are both free parameters, and $r_0 = 2.7 \pm 0.35\ h^{-1}$ Mpc when assuming $\delta = 0.8$. We derived the uncertainty on r_0 (when both A_ω and δ are free parameters) from the 68.3% confidence level obtained while fitting.

3.4. Uniformity of the sample

The mean of the angular correlation functions in each field is found to be significantly lower for stars than for galaxies; we have thus neglected the residual contributions of instrumental effects and of galactic dust across the field of view. On the other hand, following Peebles (1980, Eq. (36.6)), and assuming the mean of the ACF obtained for galaxies in each field, we found that the expected variance in counts of objects in one field is ≈29 while observations give ≈32. This leaves relatively little room for field-to-field offsets in the photometric zero points, which can artificially increase the ACF at large angular separations.

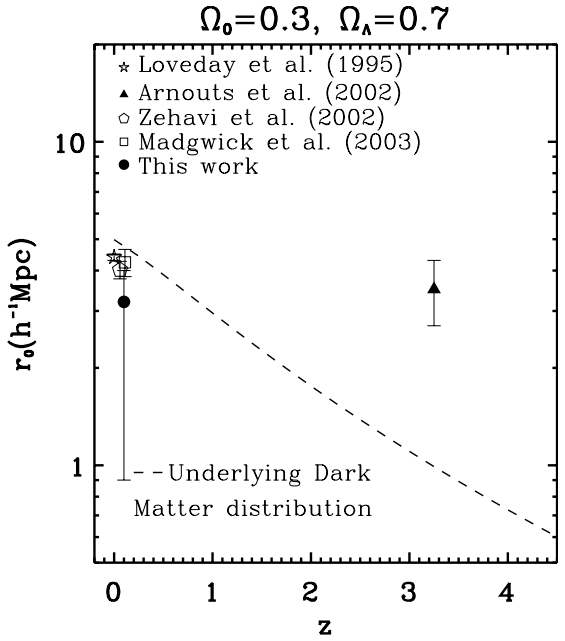

Fig. 5. The correlation lengths derived for the present UV-selected sample (filled circle), the local blue galaxies (star and pentagon symbols), the local active galaxies from 2dFGRS (open square), and the rest-frame UV-selected galaxies at $z = 3$ (filled triangle). The dashed line shows the clustering evolution of the dark matter, following Moustakas & Somerville (2002).

4. Conclusion

We have computed the angular autocorrelation function of local ($z = 0.1$) UV-selected galaxies using 3 fields from the FOCA survey. We derive a correlation length $r_0 = 3.2^{+0.8}_{-2.3}\ h^{-1}$ Mpc, comparable at the 1σ level to the correlation lengths of the active star-forming galaxies extracted from the 2dFGRS sample (Madgwick et al. 2003), of the blue galaxies from the SDSS (Zehavi et al. 2002) and of the local spiral and irregular galaxies selected in the *B*-band (Loveday et al. 1995) (Fig. 5). This correlation length is also similar to that of L_* HDF $z \approx 3$ rest-frame UV-selected galaxies (Arnouts et al. 2002) (note that $L_*(z = 3)$ is $\approx$ two magnitudes brighter than $L_*(z = 0)$, Steidel et al. 1999). Comparing these values with the underlying dark matter distribution (Moustakas & Somerville 2002) (Fig. 5) shows that L_* HDF galaxies at $z \approx 3$ are strongly biased with a typical bias parameter $b \approx 2$, while low z L_* UV galaxies appear to be unbiased or marginally anti-biased. This supports the interpretation that SF occurs preferentially in high-density regions at high z, and has spread to lower mass density regions by $z = 0$. The wealth of UV data currently collected by the GALEX mission (Martin & GALEX Science Team 2001) will allow us to pursue this investigation with high accuracy to a redshift of $\approx$1, and therefore provide crucial constraints for galaxy formation models.

Acknowledgements. We thank Todd Small for supporting the observations. We also thank Jeremy Blaizot for careful reading of the manuscript, and Tsutomu Takeuchi for useful discussions. Financial support to the FOCA balloon experiment has been provided by Centre National d'Études Spatiales and by Fonds de la Recherche Suisse.

References

Arnouts, S., Moscardini, L., Vanzella, E., et al. 2002, MNRAS, 329, 355
Bernstein, G. M. 1994, ApJ, 424, 569
Blanton, M., Cen, R., Ostriker, J. P., & Strauss, M. A. 1999, ApJ, 522, 590
Coleman, G. D., Wu, C.-C., & Weedman, D. W. 1980, ApJS, 43, 393
Cowie, L. L., Songaila, A., & Barger, A. J. 1999, AJ, 118, 603
Foucaud, S., McCracken, H. J., Le Fèvre, O., et al. 2003, A&A, 409, 835
Gómez, P. L., Nichol, R. C., Miller, C. J., et al. 2003, ApJ, 584, 210
Gal, R. R., de Carvalho, R. R., Odewahn, S. C., et al. 2003 [arXiv:astro-ph/0210298]
Giavalisco, M., & Dickinson, M. 2001, ApJ, 550, 177
Landy, S. D., & Szalay, A. S. 1993, ApJ, 412, 64
Lilly, S. J., Le Fevre, O., Hammer, F., & Crampton, D. 1996, ApJ, 460, L1
Loveday, J., Maddox, S. J., Efstathiou, G., & Peterson, B. A. 1995, ApJ, 442, 457
Madau, P., Pozzetti, L., & Dickinson, M. 1998, ApJ, 498, 106
Madgwick, D. S., Hawkins, E., Lahav, O., et al. 2003, MNRAS, 344, 847
Martin, C., & GALEX Science Team. 2001, BAAS, 33, 889
Milliard, B., Donas, J., & Laget, M. 1991, Adv. Space Res., 11, 135
Moustakas, L. A., & Somerville, R. S. 2002, ApJ, 577, 1
Nagamine, K., Cen, R., & Ostriker, J. P. 2000, ApJ, 541, 25
Peebles, P. J. E. 1980, The large-scale structure of the universe (Princeton: Princeton University Press)
Schlegel, D. J., Finkbeiner, D. P., & Davis, M. 1998, ApJ, 500, 525
Small, T. A., Sargent, W. L. W., & Hamilton, D. 1997, ApJS, 111, 1
Steidel, C. C., Adelberger, K. L., Giavalisco, M., Dickinson, M., & Pettini, M. 1999, ApJ, 519, 1
Sullivan, M., Treyer, M. A., Ellis, R. S., et al. 2000, MNRAS, 312, 442
Treyer, M. A., Ellis, R. S., Milliard, B., Donas, J., & Bridges, T. J. 1998, MNRAS, 300, 303
Yoshikawa, K., Taruya, A., Jing, Y. P., & Suto, Y. 2001, ApJ, 558, 520
Zappelli, A. 2001, Ph.D. Thesis
Zehavi, I., Blanton, M. R., Frieman, J. A., et al. 2002, ApJ, 571, 172